Experimental Method to Evaluate the Optical Properties of Aqueous Titanium Dioxide Suspensions

María L. Satuf, Rodolfo J. Brandi, Alberto E. Cassano, and Orlando M. Alfano*

INTEC, Universidad Nacional del Litoral and CONICET, Güemes 3450, S3000GLM Santa Fe, Argentina

The evaluation of the radiation field inside a slurry reactor constitutes a central step in the study of photocatalytic reactions. This task can be achieved by solving the radiative transfer equation (RTE) for the system under study. To solve the RTE, three optical properties of the catalyst suspensions are needed: the absorption coefficient, the scattering coefficient, and the phase function for scattering. In the present work, a novel experimental method to measure the optical properties of aqueous titanium dioxide (TiO_2) suspensions is proposed. The method involved diffuse reflectance and transmittance spectrophotometric measurements of the catalyst suspensions, the evaluation of the radiation field in the sample cell, and the application of a nonlinear optimization program to adjust the model predictions to the experimental data. Three commercial brands of TiO_2 were investigated: Aldrich, Degussa P25, and Hombikat UV 100.

I. Introduction

In the past decades, heterogeneous photocatalysis employing UV light and titanium dioxide (TiO_2) has received considerable attention as a method for water detoxification. Indeed, the subject has become an area of intensive research. The main advantage of photocatalysis over conventional water treatment methods is the fact that a wide range of organic compounds can be completely mineralized, leading to the formation of carbon dioxide, water, and inorganic mineral salts.

The evaluation of the radiation field inside a photoreactor constitutes a very important step in the study of photocatalytic reactions. In slurry reactors, the complexity of this task lies in the simultaneous existence of radiation absorption and scattering. A rigorous approach to obtain the spatial and directional distributions of radiation intensities is the application of the radiative transfer equation (RTE) to the system under study. To solve the RTE, three optical properties of the catalyst suspensions are required: the volumetric absorption coefficient κ_λ, the volumetric scattering coefficient σ_λ, and the phase function for scattering p.

A method to measure the absorption and scattering coefficients of TiO_2 suspensions as a function of wavelength has been proposed by Cabrera et al.[1] The extinction coefficient β_λ, defined as the sum of κ_λ and σ_λ, was also evaluated. In that work, the diffuse reflectance phase function was chosen a priori as an approximation to model the scattering effects of TiO_2 particles. Thereafter, Brandi et al.[2] modeled and experimentally verified the radiation field in a flat-plate slurry photocatalytic reactor, employing suspensions of both Aldrich and Degussa P25 TiO_2. It was shown that scattering by TiO_2 suspensions was better modeled with the isotropic phase function ($p = 1$). The specific absorption and scattering coefficients were obtained by employing the method reported by Cabrera et al.[1] but using the isotropic phase function for the parameter estimation. Subsequently, Romero et al.[3] evaluated the radiation field in an annular slurry photocatalytic reactor, using the set of parameters reported by Brandi et al.[2] The radiation spatial distribution was then verified for Aldrich and Degussa P25 TiO_2 suspensions by computing the radiative fluxes exiting the reactor and comparing these predictions with radiometer and actinometric measurements.

A number of attempts have also been made to assess the rate of absorbed photons in aqueous TiO_2 suspensions, applying different approaches. Sun and Bolton[4] determined the quantum yield for the photocatalytic generation of hydroxyl radicals in TiO_2 suspensions. The proposed method was validated using two well-known reacting systems: the photolysis of *p*-benzoquinone and hydrogen peroxide. The procedure involved the determination of the fraction of light absorbed by TiO_2 suspensions by means of a modified integrating sphere method. Other researchers applied statistical approaches to handle the coupled absorbing and scattering phenomena in heterogeneous systems. Yokota et al[5] developed a Monte Carlo simulation model to predict the photon absorption distribution in a heterogeneous photoreactor. They carried out experimental measurements of radiation transmittance and reflectance through solid particle suspensions (white silica, carbon-coated black, and white-and-black mixed particles) using a properly designed integrating sphere device attached to a spectrophotometer. Three optical parameters were defined and determined: an attenuation coefficient, a probability of radiation absorption, and a scattering parameter that was useful to determine the isotropic or anisotropic scattering mode. Salaices et al.[6,7] presented experimental methods to evaluate the rate of absorbed photons in aqueous TiO_2 suspensions in an annular photocatalytic reactor. In the first paper, the authors applied a macroscopic radiation balance to determine extinction and apparent extinction coefficients for several TiO_2 catalyst samples. In the second work, suspension extinction coefficients were determined using a radiometer with tubular black collimators, whereas the total transmitted radiation through the slurry was assessed by employing the same radiometer with tubular polished-aluminum collimators. Curcó et al.[8] proposed a model to study the effects of photon absorption and catalyst loading on the photo-

* To whom correspondence should be addressed. E-mail: alfano@intec.unl.edu.ar.

10.1021/ie050365y CCC: $30.25
Published on Web 07/06/2005

catalytic degradation of phenol and Cr(VI), employing aqueous suspensions of Degussa P25 TiO_2. Exponential and probabilistic models were used to describe the radiation propagation through the catalyst suspension. To apply these models, the authors estimated the absorption, forward scattering, and backward scattering coefficients from transmittance measurements of TiO_2 suspensions in the wavelength range 300−400 nm.

In the present work, we evaluate the absorption and scattering coefficients and the phase function of aqueous suspensions of three commercial brands of TiO_2: Aldrich, Degussa P25, and Hombikat UV 100. The main feature to be noted, as an improvement on previous work, is that the phase function is characterized from experimental data. The employed method for determining the optical properties involved diffuse reflectance and transmittance spectrophotometric measurements of TiO_2 suspensions, the evaluation of the radiation field in the spectrophotometer sample cell, and the application of a nonlinear optimization program to adjust model predictions to experimental data.

II. Extinction Coefficient

In the present paper, we make use of the specific extinction coefficient values reported in the previous work by Cabrera et al.[1] Those experimental values were obtained from absorbance spectrophotometric measurements of TiO_2 suspensions in the UV region, under specially designed conditions to minimize the collection of the scattered rays by the detector. Extinction coefficients for 6 titania brands, 5 catalyst concentrations, and 14 wavelengths in the range 275−405 nm were calculated from absorbance readings (ABS_λ) as $\beta_\lambda = 2.303ABS_\lambda/L$, where L represented the cell path length. The specific extinction coefficients β^*_λ (per unit catalyst mass concentration C_m) were obtained by applying a standard linear regression to the plots of β_λ versus C_m. These values of β^*_λ were employed in Section IV.3 to compute the scattering and absorption coefficients.

III. Diffuse Reflectance and Transmittance Measurements

The three commercial brands of TiO_2 evaluated are Aldrich (99.9+% anatase, cat. 23203−3, lot 10908DZ), Degussa P25 (~75% anatase−25% rutile, lot RV 2130), and Hombikat UV 100 (anatase, lot IF 9308/53). Cabrera et al.[1] measured the diameters of the TiO_2 particles and agglomerates for six different commercially available powders. Particle diameters (d_p) were determined in a scanning electron microscope (JEOL, model JSM35-C), whereas in situ measurements of the particle agglomerate diameters (d_a) were carried out in a laser light-scattering system (Brookhaven, model BI-9000 AT). They reported the following results: (i) Aldrich, $d_p = 150-200$ nm, $d_a = 300$ nm; (ii) Degussa P25, $d_p = 30-90$ nm, $d_a = 700$ nm; and (iii) Hombikat UV 100, $d_p = 80-100$ nm, $d_a = 900$ nm.

The aqueous suspensions for diffuse reflectance and transmittance measurements were prepared as follows: TiO_2 powders were dried in an oven at 150 °C for 12 h and then dispersed in ultrapure water. The samples were sonicated for 1 h and kept under magnetic stirring until measurement. The catalyst concentrations ranged from 0.2×10^{-3} to 2.0×10^{-3} g cm^{-3}.

The spectral diffuse reflectance and transmittance measurements of the suspensions were made by an Optronic OL series 750 spectroradiometer equipped with an OL 740-70 integrating sphere reflectance attachment. The integrating sphere, coated with poly(tetrafluoroethylene) (PTFE), has two openings in the wall for reflecting samples: the sample port and the comparison port. The detector is positioned on a port mounted on the top of the integrating sphere. The OL 740-70 attachment also contains a filter holder compartment for transmittance measurements. To work in the range of minimum instrumental error, rectangular quartz cells with an optical path of 1 mm and 5 mm were used for transmittance and reflectance measurements, respectively. Readings were made in the UV region, with wavelengths ranging from 295 to 405 nm.

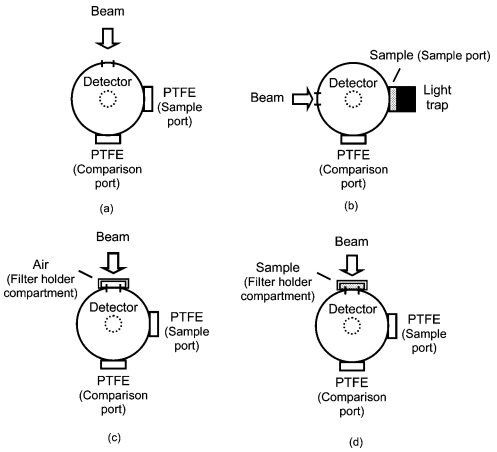

Figure 1. Integrating sphere configurations: (a) and (b), reflectance measurements; (c) and (d), transmittance measurements.

The integrating sphere configurations for measurements are schematically shown in Figure 1. For diffuse reflectance measurements, a pressed PTFE reflectance standard was used as the reference in the comparison port. 100% reflectance reading was obtained by placing another PTFE standard in the sample port (Figure 1a). To measure the reflectance of the sample, the quartz cell with the TiO_2 suspension was placed in the sample port with its back covered by a light trap that absorbs all transmitted radiation, keeping the PTFE standard in the comparison port (Figure 1b). For diffuse transmittance measurements, PTFE reflectance standards were placed in the comparison and sample ports of the sphere. 100% transmittance reading was obtained against air (Figure 1c). To measure the transmittance of the sample, the cell with the catalyst suspension was placed in the filter holder compartment (Figure 1d).

IV. Radiation Field Model

IV.1. Radiative Transfer Equation. The RTE describes the radiation intensity I_λ at any position along a ray path through a medium. This equation can be applied to evaluate the radiation field in the heterogeneous system constituted by TiO_2 particulate suspensions in water. For a participating medium, with absorption and scattering (no emission is considered), the RTE can be written as

$$\frac{dI_\lambda(s,\underline{\Omega})}{ds} + \beta_\lambda I_\lambda(s,\underline{\Omega}) = \frac{\sigma_\lambda}{4\pi}\int_{\Omega'=4\pi} p(\underline{\Omega}'\cdot\underline{\Omega}) I_\lambda(s,\underline{\Omega}')\, d\Omega' \quad (1)$$

The right-hand side of eq 1 represents the gain of radiant energy along the direction $\underline{\Omega}$ due to the incoming scattering from all directions ($\underline{\Omega}'$). More specifically,

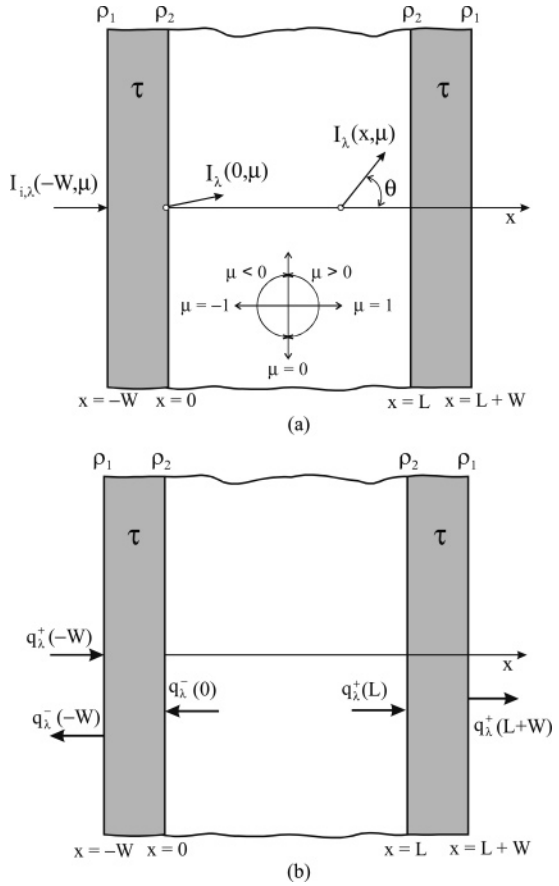

Figure 2. Schematic representation of the spectrophotometer cell: (a) coordinate system for the one-dimensional, one-directional radiation model; (b) inlet and outlet radiative fluxes.

the phase function $p(\underline{\Omega}'\cdot\underline{\Omega})$ represents the probability that the incident radiation from direction $\underline{\Omega}'$ will be scattered and incorporated into direction $\underline{\Omega}$. This term gives the RTE its integro-differential nature and is responsible for most of the difficulties associated with its numerical integration.

The rectangular spectrophotometer cell, employed for reflectance and transmittance measurements, can be represented as an infinite plane parallel medium with azimuthal symmetry, as shown in Figure 2. Then, a one-dimensional, one-directional radiation transport model was applied to solve the RTE in the cell; that is,

$$\frac{\mu}{\beta_\lambda}\frac{\partial I_\lambda(x,\mu)}{\partial x} + I_\lambda(x,\mu) = \frac{\omega_\lambda}{4\pi}\int_{\mu'=-1}^{1} I_\lambda(x,\mu')\int_{\phi'=0}^{2\pi} p(\mu_0)\,\mathrm{d}\phi'\,\mathrm{d}\mu' \quad (2)$$

where $\omega_\lambda = \sigma_\lambda/\beta_\lambda$ is the spectral albedo, defined as the ratio of the scattering coefficient to the extinction coefficient; x is the axial coordinate; μ is the direction cosine; and μ_0 is the cosine of the scattering angle θ_0 between the directions of the incident and scattered rays.

The phase function p can be expanded in the form[9]

$$p(\mu_0) = \sum_{n=0}^{N} a_n P_n(\mu_0), \quad a_0 = 1 \quad (3)$$

where $P_n(\mu_0)$ are the Legendre polynomials of order n and argument μ_0 and a_n are the corresponding expansion coefficients. For systems with azimuthal symmetry, integrating the phase function over ϕ' from 0 to 2π gives

$$\int_{\phi'=0}^{2\pi} p(\mu_0)\,\mathrm{d}\phi' = 2\pi\sum_{n=0}^{N} a_n P_n(\mu)P_n(\mu') = 2\pi p(\mu,\mu') \quad (4)$$

Introducing eq 4 in eq 2 yields

$$\frac{\mu}{\beta_\lambda}\frac{\partial I_\lambda(x,\mu)}{\partial x} + I_\lambda(x,\mu) = \frac{\omega_\lambda}{2}\int_{\mu'=-1}^{1} I_\lambda(x,\mu')p(\mu,\mu')\,\mathrm{d}\mu' \quad (5)$$

It is worth noting that, in a purely absorbing medium (not including emission or scattering), $\omega_\lambda = 0$ and eq 5 can be reduced to the Beer−Lambert law, which is the basis of conventional spectrophotometric measurements for homogeneous systems.

The boundary conditions for eq 5 (at $x = 0$ and $x = L$ in Figure 2) must account for the optical effects of the cell walls, namely, absorption, refraction, and multiple reflection. Because of the relatively small thickness of the sample cell wall, and in order to simplify calculations, the contribution of refraction was neglected. Consequently, the net radiation method[10] has been applied to model the two major effects: absorption and reflection. Therefore, considering the quartz walls of the cell as specularly reflecting surfaces, the boundary conditions take the following form (Figure 2a):

$$I_\lambda(0,\mu) = Y_{\mathrm{W},\lambda} I_{\mathrm{i},\lambda}(-W,\mu) + \Gamma_{\mathrm{W2},\lambda} I_\lambda(0,-\mu) \qquad (\mu > 0) \quad (6)$$

$$I_\lambda(L,\mu) = \Gamma_{\mathrm{W2},\lambda} I_\lambda(L,-\mu) \qquad (\mu < 0) \quad (7)$$

where $Y_{\mathrm{W},\lambda}$ is the global wall transmission coefficient and $\Gamma_{\mathrm{W2},\lambda}$ represents the global wall reflection coefficient corresponding to the radiation that arrives from the internal side of the cell. These coefficients can be calculated from[2]

$$Y_{\mathrm{W},\lambda} = \frac{(1-\rho_2)(1-\rho_1)\tau}{1-\rho_1\rho_2\tau^2} \quad (8)$$

$$\Gamma_{\mathrm{W2},\lambda} = \frac{\rho_2 - 2\rho_1\rho_2\tau^2 + \rho_1\tau^2}{1-\rho_1\rho_2\tau^2} \quad (9)$$

Here, ρ_1 and ρ_2 are the interface reflectivities (air−quartz and quartz−suspension, respectively), which can be calculated by using Snell's law and Fresnel's equations, and τ represents the internal transmittance of the quartz wall. Strictly speaking, the global coefficients given by eqs 8 and 9 are dependent on the direction of the incident rays at the cell wall. As an approximation, one can use global coefficients averaged over all possible directions; an alternative approach is to evaluate these coefficients experimentally. In this sense, the global reflection and transmission coefficients employed in the present work were experimentally assessed by means of diffuse spectrophotometric measurements of the cell filled with ultrapure water.

IV.2. Phase Function. The choice of the phase function p represents an important step in any calculation where multiple scattering is involved. It should be noted that, in a well-defined physical problem, the phase function is given, not chosen.[11] However, complicated functions lead to very time-consuming computations. It

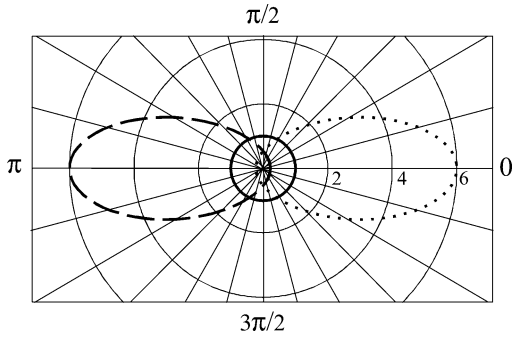

Figure 3. $p_{HG,\lambda}$ vs θ_0 for different values of g_λ: solid line, $g_\lambda = 0.0$; broken line, $g_\lambda = -0.5$; dotted line, $g_\lambda = 0.5$.

is then a common practice to employ a phase function that preserves the main characteristics of the actual function and still renders the multiple-scattering computations manageable.

The Henyey and Greenstein (HG) phase function ($p_{HG,\lambda}$) is characterized by[10]

$$p_{HG,\lambda}(\mu_0) = \frac{(1 - g_\lambda^2)}{(1 + g_\lambda^2 - 2g_\lambda\mu_0)^{3/2}} \tag{10}$$

where g_λ is the dimensionless asymmetry factor, defined as

$$g_\lambda = \frac{1}{2}\int_{-1}^{1} p_{HG,\lambda}(\mu_0)\mu_0 \, d\mu_0 \tag{11}$$

and the Legendre expansion coefficients are given by

$$a_n = (2n + 1)g_\lambda^n \tag{12}$$

Notice that the dimensionless asymmetry factor can be a function of wavelength. Consequently, $p_{HG,\lambda}$ can also have a dependence on the radiation wavelength. It should also be noted that $p_{HG,\lambda}$ is determined by a single free parameter (g_λ) that varies smoothly from isotropic ($g_\lambda = 0$) to a narrow forward peak ($g_\lambda = 1$) or to a narrow backward peak ($g_\lambda = -1$). Figure 3 shows the plots of $p_{HG,\lambda}$ versus θ_0, in polar coordinates, for three arbitrary values of the asymmetry factor: −0.5, 0.0, and 0.5.

The knowledge of g_λ alone suffices to obtain solutions of multiple scattering problems with a high grade of accuracy, making the $p_{HG,\lambda}$ ideal for calculations.[11] For the reasons formerly mentioned, we have chosen the $p_{HG,\lambda}$ as the phase function for the radiation model in the sample cell.

To solve eqs 5−7, the discrete ordinate method[12] was applied. This method transforms the RTE into a set of algebraic equations that can be solved numerically. It should be pointed out that ω_λ and g_λ remain as unknown parameters. In other words, we are facing an inverse analysis of radiative transfer, where the optical properties will be determined from a set of measured radiation quantities.[13]

IV.3. Parameters Estimation. To compare the model predictions with the diffuse reflectance and transmittance measurements, we should interpret results in terms of net radiative fluxes. The spectral net radiative flux, $q_\lambda(x)$, for the one-dimensional, one-directional model with azimuthal symmetry can be written as

$$q_\lambda(x) = 2\pi\int_\mu I_\lambda(x,\mu)\mu \, d\mu \tag{13}$$

Accordingly, considering Figure 2b, diffuse reflectance and transmittance values can be interpreted as the ratio between net radiative fluxes:

$$R_\lambda = \frac{q_\lambda^-(-W)}{q_\lambda^+(-W)} \tag{14}$$

$$T_\lambda = \frac{q_\lambda^+(L+W)}{q_\lambda^+(-W)} \tag{15}$$

where

$$q_\lambda^-(-W) = 2\pi\int_{\mu=-1}^{0} I_\lambda(-W,\mu)\mu \, d\mu \tag{16}$$

$$q_\lambda^+(-W) = 2\pi\int_{\mu=0}^{1} I_{i,\lambda}(-W,\mu)\mu \, d\mu \tag{17}$$

$$q_\lambda^+(L+W) = 2\pi\int_{\mu=0}^{1} I_\lambda(L+W,\mu)\mu \, d\mu \tag{18}$$

Reflectance and transmittance model predictions are calculated with the values of I_λ obtained from the solution of the RTE (eqs 5−7). However, these values represent the radiation intensities at the inner walls ($x = 0$ and $x = L$). Therefore, to compare theoretical results with experimental results, one must account for the effect of the cell walls and obtain the corresponding values at $x = -W$ and $x = L + W$. The approach employed to calculate the intensities outside the sample cell is similar to the one applied for the boundary conditions

$$I_\lambda(-W,\mu) = Y_{W,\lambda}I_\lambda(0,\mu) + \Gamma_{W1,\lambda}I_{i,\lambda}(-W,-\mu) \qquad (\mu < 0) \tag{19}$$

$$I_\lambda(L+W,\mu) = Y_{W,\lambda}I_\lambda(L,\mu) \qquad (\mu > 0) \tag{20}$$

where $\Gamma_{W1,\lambda}$ represents the global wall reflection coefficient corresponding to the radiation that arrives from the external side of the cell. $\Gamma_{W1,\lambda}$ is calculated as

$$\Gamma_{W1,\lambda} = \frac{\rho_1 - 2\rho_1\rho_2\tau^2 + \rho_2\tau^2}{1 - \rho_1\rho_2\tau^2} \tag{21}$$

A nonlinear, multiparameter regression procedure (a modified Levenberg−Marquardt method) was applied to adjust theoretical values to experimental information. The optimization program renders the values of ω_λ and g_λ that minimize the differences between model predictions and experimental data. Then, for each concentration of TiO_2 and each wavelength, the volumetric scattering and absorption coefficients were obtained as

$$\sigma_\lambda = \beta_\lambda\omega_\lambda \tag{22}$$

$$\kappa_\lambda = \beta_\lambda - \sigma_\lambda \tag{23}$$

The specific absorption and scattering coefficients ($\kappa_\lambda^* = \kappa_\lambda/C_m$ and $\sigma_\lambda^* = \sigma_\lambda/C_m$), calculated per unit catalyst mass concentration, were obtained by applying a standard linear regression on the data κ_λ versus C_m and σ_λ versus C_m, respectively. Figure 4 shows the regression plots of the scattering coefficients for the three tested catalysts and for three different wavelengths (λ = 345, 365, and 385 nm). The corresponding linear regression coefficients are also depicted in the figure.

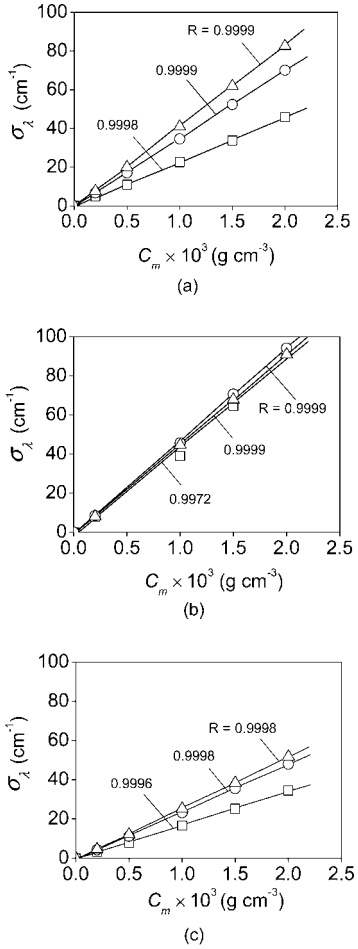

Figure 4. Linear regression plots for scattering coefficients: (a) Aldrich; (b) Degussa P25; (c) Hombikat UV 100. Keys: □, 345 nm; ○, 365 nm; △, 385 nm.

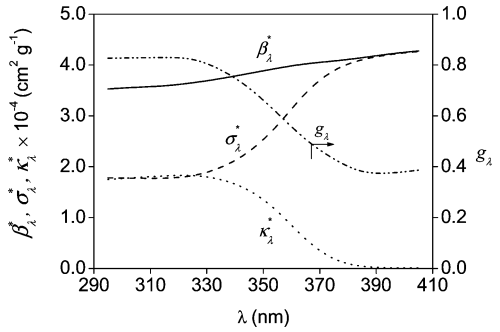

Figure 5. Optical properties vs wavelength for Aldrich catalyst: solid line, β_λ^*; broken line, σ_λ^*; dotted line: κ_λ^*; broken and dotted line, g_λ.

The values of the dimensionless asymmetry factor, for each wavelength, were obtained by calculating the average value of g_λ for all the C_m tested in the experimental work.

V. Analysis of the Results

Figures 5−7 show the calculated optical properties for the three investigated brands of TiO_2: Aldrich, Degussa P25, and Hombikat UV 100. The specific absorption, scattering, and extinction coefficients, as well as the dimensionless asymmetry factor to represent the phase function, are plotted as a function of wavelength. As mentioned before, the values of the specific

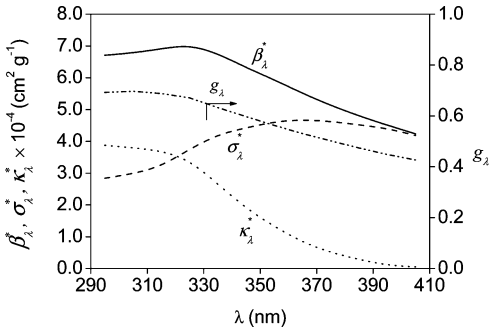

Figure 6. Optical properties vs wavelength for Degussa P25 catalyst: solid line, β_λ^*; broken line, σ_λ^*; dotted line: κ_λ^*; broken and dotted line, g_λ.

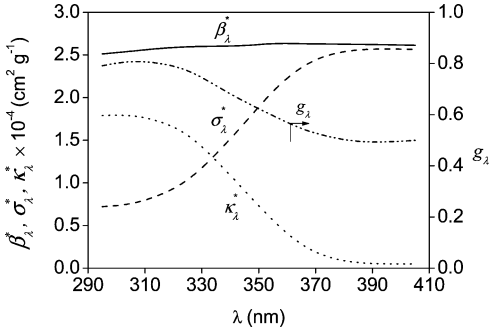

Figure 7. Optical properties vs wavelength for Hombikat UV 100 catalyst: solid line, β_λ^*; broken line, σ_λ^*; dotted line: κ_λ^*; broken and dotted line, g_λ.

extinction coefficients depicted in these figures are those reported by Cabrera et al.[1]

The specific absorption coefficients corresponding to the Aldrich sample decrease to almost 0 at 385 nm, which is approximately the theoretical value corresponding to the band gap of the semiconductor (∼3.2 eV). The Degussa P25 and Hombikat UV 100 samples still show a slight absorption beyond 385 nm, a fact that can be explained by the absorption of some catalyst impurities. Comparing the absorption coefficients for the three commercial brands, the values of κ_λ^* for Degussa P25 are higher than those corresponding to Aldrich and Hombikat UV 100 over the whole range of wavelengths, especially <330 nm, where the values for Degussa are about two times larger. It can also be noted that the specific scattering coefficients are higher for the Degussa P25 catalyst.

Analyzing the values of the absorption and the scattering coefficients for each sample, we found that, for short wavelengths, κ_λ^* appears to be comparable or even larger than σ_λ^*, depending on the type of catalyst being considered. For example, for $\lambda < 320$ nm, the values of $\kappa_\lambda^* \approx \sigma_\lambda^*$ for the Aldrich catalyst (albedo ≈ 0.5). On the other hand, $\kappa_\lambda^* > \sigma_\lambda^*$ (albedo < 0.5) for the Degussa P 25 and Hombikat UV 100 catalysts. It is worth noting that this behavior for short wavelengths is different than that reported by Cabrera et al.;[1] in the wavelength range between 275 and 405 nm, they found that the specific absorption coefficients were always lower than the corresponding scattering coefficients. This difference is a direct consequence of the adopted phase function.

With regard to the asymmetry factor g_λ, its spectral distribution is similar for Aldrich and Hombikat samples, with lower values ∼380−400 nm and higher values ∼300 nm (Figures 5 and 7). The qualitative behavior of

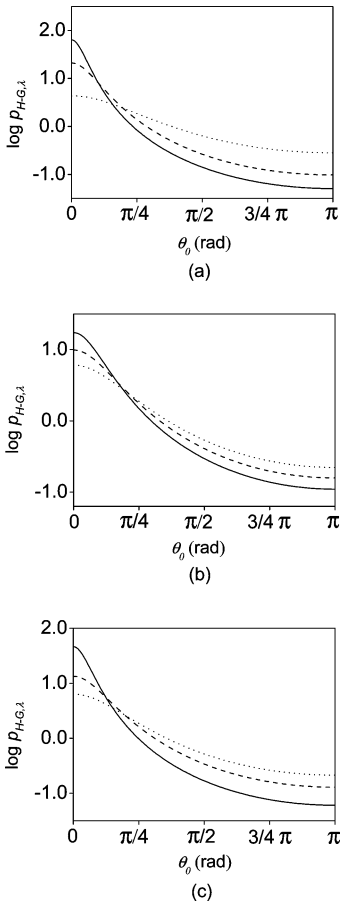

Figure 8. log $p_{HG,\lambda}$ vs θ_0: (a) Aldrich; (b) Degussa P25; (c) Hombikat UV 100. Keys: solid line, 315 nm; broken line, 345 nm; dotted line, 375 nm.

g_λ for the Degussa sample is slightly different from those of the other brands, with a smoother variation over the spectral range (Figure 6). It should be remarked that values of g_λ are positive over the whole range of wavelengths for the three tested catalysts, ranging from 0.4 to 0.8, approximately. This behavior indicates a preferential forward direction of the scattered rays over titania particulate suspensions.

For each catalyst brand, Figure 8 shows the plots of log $p_{HG,\lambda}$ versus θ_0 for three characteristic wavelengths: 315, 345, and 375 nm. Notice that a higher angular anisotropy is observed at the lower wavelengths. For example, for the Aldrich brand and $\lambda = 315$ nm, $p_{HG,\lambda}$ in the forward direction ($\theta_0 = 0$) is ~3 orders of magnitude higher than that in the backward direction ($\theta_0 = \pi$). On the other hand, for the same photocatalyst and $\lambda = 375$ nm, $p_{HG,\lambda}$ at $\theta_0 = 0$ is only 1 order of magnitude higher than the corresponding phase function at $\theta_0 = \pi$.

For the three characteristic wavelengths ($\lambda = 315$, 345, and 375 nm) and for Degussa P25, let us compare the specific absorption coefficients estimated from (i) the diffuse phase function,[1] (ii) the isotropic phase function,[2,3] and (iii) the HG phase function, computed with the asymmetry factors reported in Figure 6 (this work). Values of κ_λ^* for the three cases are reported in Table 1. It is important to note that the specific absorption coefficients obtained with the HG phase function are ca. 2−3 times larger than those obtained in previous work employing the diffuse phase function or the isotropic phase function. These results clearly show that the knowledge of the phase function p is an important step to estimate the optical properties of TiO_2 suspensions and, from the values of these optical parameters, to compute the absorbed radiation distribution inside a heterogeneous reacting system.

Table 1. Degussa P 25 Specific Absorption Coefficients Obtained with Different Phase Functions

	κ_λ^* (cm^2 g^{-1})		
λ (nm)	diffuse[1]	isotropic[2,3]	HG[a]
315	11620	18722	37062
345	4485	8082	18886
375	0	1293	5013

[a] This work.

VI. Conclusions

A novel experimental method has been developed to measure the optical properties of aqueous TiO_2 suspensions as a function of wavelength. These properties (the absorption and scattering coefficients and the phase function for scattering) are necessary to solve the RTE for a heterogeneous system and to compute the rate of photon absorption inside a photocatalytic reactor. The absorption and scattering coefficients were estimated as specific properties (per unit catalyst mass concentration). The phase function was determined by employing a single free parameter: the dimensionless asymmetry factor.

The employed method was based on diffuse reflectance and transmittance measurements of TiO_2 suspensions, the solution of the RTE inside the sample cell, and the application of a nonlinear, multiparameter regression procedure to adjust the model predictions to the experimental data. Three different brands of TiO_2 were investigated: Aldrich, Degussa P25, and Hombikat UV 100.

It was found that, for short wavelengths ($\lambda \leq 320$ nm), the specific absorption coefficient can be comparable (Aldrich brand) or even larger (Degussa P25 and Hombikat UV 100 brands) than the specific scattering coefficient.

As an improvement on previous work, the parameter of the adopted phase function was estimated from experimental measurements. We found that the values of the asymmetry factor for the three investigated catalysts were positive in the wavelength range from 295 to 405 nm, indicating a preferential forward direction of the scattered rays over titania particulate suspensions. At lower wavelengths, a higher angular anisotropy was observed; values of the phase function in the forward direction were up to 3 orders of magnitude higher than those in the backward direction. Conversely, at higher wavelengths, a lower angular anisotropy was observed.

The optical properties were determined from measurements of very small volumes of uniform suspensions in order to relate these values with the corresponding catalyst concentration; then, the proposed approach was able to produce quasi-point values of the specific coefficients (per unit catalyst mass concentration). As a result, these coefficients depend only on the radiation wavelength. Therefore, knowing the spatial and temporal variation of the catalyst concentration in a real photocatalytic reactor, the reported optical properties can be readily used to compute the photon absorption rate.

Acknowledgment

The authors are grateful to Universidad Nacional del Litoral (UNL), Consejo Nacional de Investigaciones Científicas y Técnicas (CONICET), and Agencia Nacional de Promoción Científica y Tecnológica (ANPCyT) for the financial support. They also thank Antonio C. Negro for his valuable help during the experimental work and Claudia M. Romani for her technical assistance.

Supporting Information Available: Tables reporting the values of κ_λ^*, σ_λ^*, and g_λ for the three investigated catalysts. This material is available free of charge via the Internet at http://pubs.acs.org.

Nomenclature

a_n = expansion coefficient of order n
d_a = catalyst agglomerate diameter (nm)
d_p = catalyst particle diameter (nm)
C_m = catalyst mass concentration (g cm^{-3})
g = asymmetry factor (dimensionless)
I = radiation intensity (einstein cm^{-2} sr^{-1} s^{-1})
L = cell path length (cm)
P_n = Legendre polynomial of order n
p = phase function (dimensionless)
q = radiative flux (einstein cm^{-2} s^{-1})
s = linear coordinate along the direction Ω (cm)
W = cell wall thickness (cm)
x = axial coordinate (cm)

Greek Letters

β = volumetric extinction coefficient (cm^{-1})
β^* = specific extinction coefficient (cm^2 g^{-1})
Γ = global reflection coefficient (dimensionless)
θ = spherical coordinate (rad)
θ_0 = angle between the direction of the incident and the scattered rays (rad)
κ = volumetric absorption coefficient (cm^{-1})
κ^* = specific absorption coefficient (cm^2 g^{-1})
λ = wavelength (nm)
μ = direction cosine of the ray for which the RTE is written
μ' = direction cosine of an arbitrary ray before scattering
μ_0 = cosine of the angle θ_0
ρ = interface reflectivity (dimensionless)
σ = volumetric scattering coefficient (cm^{-1})
σ^* = specific scattering coefficient (cm^2 g^{-1})
τ = cell wall internal transmittance (dimensionless)
Υ = global transmission coefficient (dimensionless)
φ = spherical coordinate (rad)
ω = albedo (dimensionless)
$\underline{\Omega}$ = unit vector in the direction of radiation propagation
$\overline{\Omega}$ = solid angle (sr)

Superscripts

+ = forward direction
− = backward direction

Subscripts

i = inlet condition
W = relative to the cell wall
λ = dependence on wavelength
1 = relative to the external side of the cell wall (air−quartz interface)
2 = relative to the internal side of the cell wall (quartz−suspension interface)

Literature Cited

(1) Cabrera, M. I.; Alfano, O. M.; Cassano, A. E. Absorption and Scattering Coefficients of Titanium Dioxide Particulate Suspensions in Water. *J. Phys. Chem.* **1996**, *100*, 20043.

(2) Brandi, R. J.; Alfano, O. M.; Cassano, A. E. Rigorous Model and Experimental Verification of the Radiation Field in a Flat-Plane Solar Collector Simulator Employed for Photocatalytic Reactions. *Chem. Eng. Sci.* **1999**, *54*, 2817.

(3) Romero, R. L.; Alfano, O. M.; Cassano, A. E. Radiation Field in an Annular, Slurry Photocatalytic Reactor. 2. Model and Experiments. *Ind. Eng. Chem. Res.* **2003**, *42*, 2479.

(4) Sun, L.; Bolton, J. R. Determination of the Quantum Yield for the Photochemical Generation of Hydroxyl Radicals in TiO_2 Suspensions. *J. Phys. Chem.* **1996**, *100*, 4127.

(5) Yokota, T.; Cesur, S.; Suzuki, H.; Baba, H.; Takahata, Y. Anisotropic Scattering Model for Estimation of Light Absorption Rates in Photoreactor with Heterogeneous Medium. *J. Chem. Eng. Jpn.* **1999**, *32*, 314.

(6) Salaices, M.; Serrano, B.; de Lasa, H. I. Photocatalytic Conversion of Organic Pollutants. Extinction Coefficients and Quantum Efficiencies. *Ind. Eng. Chem. Res.* **2001**, *40*, 5455.

(7) Salaices, M.; Serrano, B.; de Lasa, H. I. Experimental Evaluation of Photon Absorption in an Aqueous TiO_2 Slurry Reactor. *Chem. Eng. J.* **2002**, *90*, 219.

(8) Curcó, D.; Giménez, J.; Addardak, A.; Cervera-March, S.; Esplugas, S. Effects of radiation absorption and catalyst concentration on the photocatalytic degradation of pollutants. *Catal. Today*. **2002**, 76, 177.

(9) Özisik, M. N. *Radiative Transfer and Interactions with Conduction and Convection*; Wiley: New York, 1973.

(10) Siegel, R.; Howell, J. R. *Thermal Radiation Heat Transfer*, 4th ed.; Hemisphere Publishing Corp.: Bristol, PA, 2002.

(11) Van de Hulst, H. C. *Multiple Light Scattering*; Academic Press: New York, 1980.

(12) Duderstadt, J. J.; Martin, W. R. *Transport Theory*; Wiley: New York, 1979.

(13) Ho, C. H.; Özisik, M. N. An Inverse Radiation Problem. *Int. J. Heat Mass Transfer* **1989**, *32*, 335.

Received for review March 19, 2005
Revised manuscript received May 17, 2005
Accepted June 2, 2005

IE050365Y